NUMERICAL ANALYSIS OF A HYDROFOIL IN CLOSE PROXIMITY TO

FREE SURFACE

MURAT AYYILDIZ

PÎRÎ REİS UNIVERSITY

2019

NUMERICAL ANALYSIS OF A HYDROFOIL IN CLOSE PROXIMITY TO FREE SURFACE

MURAT AYYILDIZ

PÎRÎ REİS UNIVERSITY

2019

NUMERICAL ANALYSIS OF A HYDROFOIL IN CLOSE PROXIMITY TO FREE SURFACE

Murat AYYILDIZ

M.Sc., Naval Architecture and Marine Engineering - High Performance Marine Platforms, Pîrî Reis University 2019

Submitted to the Institute for Graduate Studies in Science and Engineering in partial fulfillment of the requirements for the degree of Master of Science

Graduate Program in Naval Architecture and Marine Engineering - High Performance Marine Platforms Pîrî Reis University

2019

Murat AYYILDIZ, M.Sc. student of Pîrî Reis University Naval Architecture and Marine Engineering-High Performance Ocean Platforms student ID 168017007, successfully defended the thesis entitled "NUMERICAL ANALYSIS OF A HYDROFOIL IN CLOSE PROXIMITY TO FREE SURFACE" which he prepared after fulfilling the requirements specified in the associated legislations, before the jury whose signatures are below.
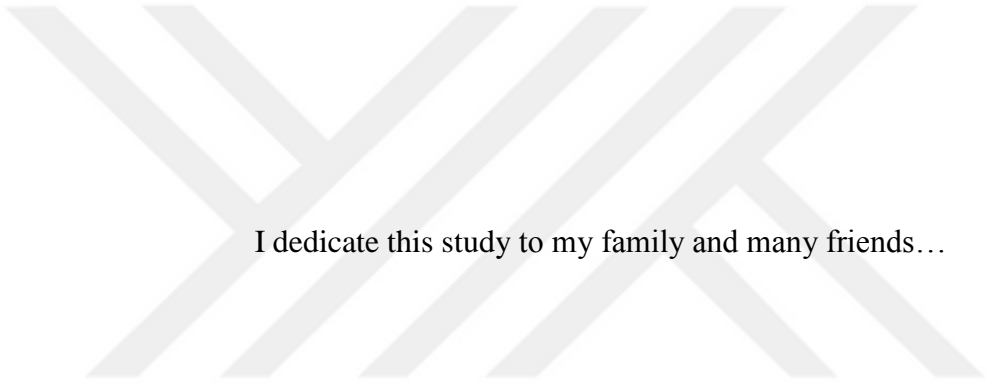
SUPERVISIORS

Dr. A. Ziya SAYDAM……………......………………………………………….....................

Dr. Murat ÖZBULUT ……………......…………………………………………………..

APPROVED BY

Prof. M. Sander ÇALIŞAL……………......…………………………………………………..

Prof. Ömer GÖREN……………………………………………………………………....

Assoc.Prof. D. Bülent DANIŞMAN……………......………………………………………

DATE OF APPROVAL:24.05.2019

I dedicate this study to my family and many friends…

ACKNOWLEDGEMENTS

TABLE OF CONTENTS

ABBREVIATIONS

CAD	Computer-Aided Design
CFD	Computational Fluid Dynamics
EFD	Experimental Flow Data
ITTC	International Towing Tank Conference
NACA	National Advisory Committee for Aeronautics
RANS	Reynolds-Averaged Navier-Stokes
SPH	Smoothed Particle Hydrodynamics
SST	Shear Stress Transport
TKE	Turbulent Kinetic Energy

LIST OF TABLES

Tables

LIST OF FIGURES

Figures

NOMENCLATURE

AR	Aspect Ratio
C	Chord Length
CD	Drag Coefficient
CL	Lift Coefficient
D	Drag Force
$\emptyset(x, y, z; t)$	perturbation potential
∇	free surface
B	beam
D	depth
F_b	Initial buoyancy force
Fr	Froude Number
g	acceleration due to gravity
h	draft
kn	knot
kN	kilo Newton
l	position of the hydrofoil x axis
L	length
m	meter
pi	order of accuracy
R_i	convergence ratio
r_i	uniform refinement ratio
Re	Reynolds Number

RE	Richardson Extrapolation
S	Planform area in hydrofoil
S_{Gi}	solution of grid analysis
S_{Ti}	solution of time analysis
s	second
U	flow velocity
U_D	Experimental uncertainty
U_G	Grid uncertainty
U_T	Time step uncertainty
U_{SN}	Verification uncertainty
U_V	Validation uncertainty
x,y,z	longitudinal, transverse and vertical position of the section
$\Phi(x, y, z; t)$	velocity potential
ζ	wave amplitude
ρ	fluid density

ABSTRACT

NUMERICAL ANALYSIS OF A HYDROFOIL IN CLOSE PROXIMITY TO FREE SURFACE

In this study, the hydrodynamic and wave making characteristics of a submerged hydrofoil has been evaluated by numerical techniques. Experimental data available for different depths of submergence and flow velocities have been compared to the results obtained by a commercial RANS CFD code. The capabilities of the numerical approaches in terms of capturing the free surface deformation have been assessed. At high Froude numbers, the induced wave profiles have been observed to exhibit an unsteady nature by RANS numerical method.

The uncertainty of the RANS package has also been analyzed for wave amplitude and wave resistance. RANS numerical technique has been validated in terms of the investigated hydrodynamic parameters. Hydrodynamic performance of the submerged hydrofoil variation of lift and drag with Froude number has also been assessed by RANS numerical technique.

Keywords: Open Channel flow, CFD, Uncertainty, RANS, Hydrofoil, Free Surface Hydrodynamics

ÖZET

SERBEST SU YÜZEYİNE YAKIN BİR HİDROFOİLİN NUMERİK OLARAK İNCELENMESİ

Bu çalışmada, serbest su yüzeyine yakın bir hidrofoilin hidrodinamik ve dalga yapma karakteristikleri sayısal tekniklerle değerlendirililmiştir. Deney sonuçları farklı derinlikler ve akış hızlarında RANS hesaplamalı akışkanlar dinamiği kodu ile karşılaştırılmıştır. Sayısal yaklaşımların serbest su yüzeyi deformasyonunun tahmini açısından kabiliyetleri değerlendirilmiştir. Özellikle yüksek Froude sayılarında, indüklenen dalga profillerinin, her yüksek mertebede zamana bağlı (kararsız) bir doğası olduğu gözlemlenmiştir.

Akışın kararsız bir yapıya sahip olduğu RANS yöntemi ile görülmüştür. RANS analizlerinin belirsizliği, dalga genliği ve dalga direnci açısından da analiz edilmiştir. RANS sayısal tekniğinin belirisizliği incelenen hidrodinamik parametreler açısından doğrulanmıştır. Serbest su yüzeyine yakın hidrofoil hidrodinamik performansı da RANS sayısal tekniği ile değerlendirilmiştir.

Anahtar Kelimeler: Açık Kanal Akışı,HAD,Belirsizlik,RANS,Hidrofoil,Serbest Su Yüze

1. INTRODUCTION

The hydrodynamics of submerged bodies are vital areas of investigation in naval architecture and fluid dynamics. Wave resistance prediction is an important problem for the ship designers. The wave breaking resistance is especially important for cases with breaking of the wave. The energy transmitted to the water by wave breakage is equal to the wave breaking resistance of the ship and in certain cases it will play an important role in determining the total resistance of the ship. The investigation of flow around a submerged body in close proximity to the free-surface has an huge importance for the design procedures of many marine science applications like hydrofoils in sailing yachts, wave resistance calculations of a ship, offshore structures, bulb design of a ship, submarines, water-based power generation systems and construction of underwater pipelines[1,2,3,4].

In recent years, computational fluid dynamics methods have gained popularity in the field of numerical hydrodynamics. The numerical simulation is a promising feature for hydrodynamics. There are innumerable experimental studies that may be utilized as validation cases for numerical techniques. Researchers have primarily used potential methods, RANS CFD and Smoothed Particle Hydrodynamics (SPH) for investigation of the performance of submerged bodies[5,6,7]. In this study, the flow around to hydrofoil close proximity to free-surface will be investigated by the RANS numerical techniques.

1.1 Aims of the Project

The main objective of the present work is to investigate the capability of numerical approaches in estimating the flow around a submerged hydrofoil in close proximity to free surface , mainly by mesh-based Reynolds Averaged Navier-Stokes (RANS). Free surface deformations behind the profile will be compared with the experimental data from the literature for two submergence levels of the profile and three different Froude numbers for each level. Investigation of wave resistance and hydrodynamic performance characteristics of the immersed hydrofoil for one submergence level and several flow velocities will also be conducted. Verification and validation uncertainty in the prediction of wave profiles and wave resistance will be quantified for mesh-based Reynolds Averaged Navier-Stokes (RANS).

1.2 Methodology

In this section, the content of the study is going to be presented consecutively.

Chapter 2 summarizes the numerical definitions associated with the free surface hydrodynamics, examination of studies in literature about flow around a submerged body in the free surface and describes uncertainty analysis procedure used for the problem.

Chapter 3 including the rendetion of relative numerical results with the findings of Salvesen (1969) in the following manner: The free-surface deformations acquired from RANS simulations, the validation of RANS model wave resistance analyses and the examination of hydrodynamic performance characteristics of the submerged hydrofoil and the execution of uncertainty analysis procedure based on the the problem.

Discussions remarks will be drawn in Chapter 4.

Chapter 5 represents conclusion, further studies and suggestions.

2. THEORETICAL BACKGROUND

2.1 Free Surface Hydrodynamics

The waves actually progress in a viscous fluid over a floor having irregular and variable permeability. After all most of the time fluid movement is almost irrotational. The reason for this is that the viscous effects are usually thin on the surface and near the floor is the concentration of "boundary layers". Water can also be considered as an incompressible liquid, there are potential and available functions in the waves.[8]
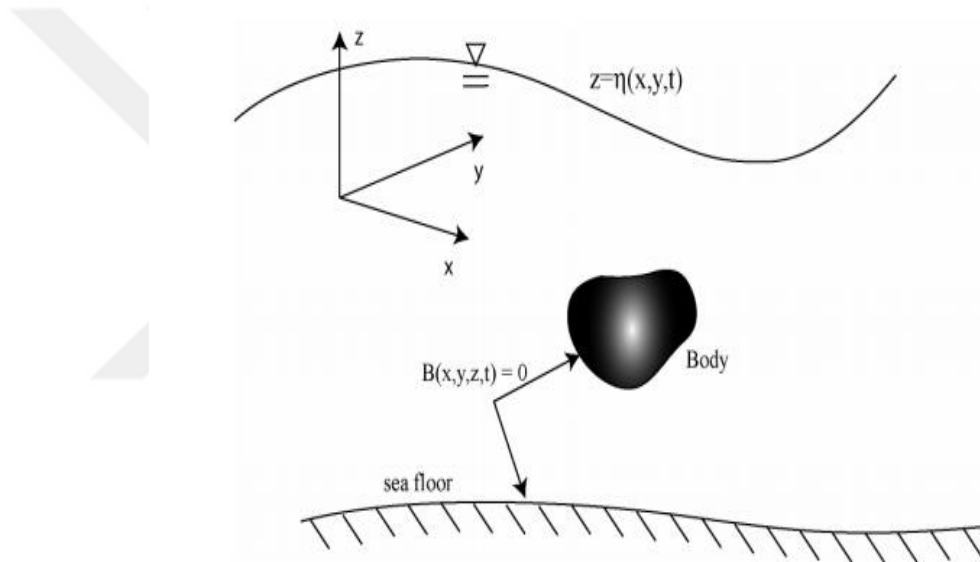
Figure 2.1 Free Surface Water Wave Problem[9]

The linear wave theory is a simple boundary value problem of potential theory. The solutions to be obtained must realize the boundary conditions in wave motion. These boundary conditions; Bottom boundary condition, free surface dynamic boundary condition, free surface kinematic boundary condition.[8]

The equation of motion for an ideal fluid with an incompressible inviscid is shown

$$\frac{dV}{dt} = F - \frac{1}{p} \nabla p \qquad (2.1)$$

above. Else

4

$$\frac{dV}{dt} = \frac{\partial V}{\partial t} + \frac{1}{2}\nabla V^2 - V \wedge (\nabla \wedge V) \qquad (2.2)$$

has been written. $\nabla \wedge V = \Omega$ movement is rotational

$$\frac{\partial V}{\partial t} + \frac{1}{2}\nabla V^2 - V \wedge \Omega = F - \frac{1}{p}\nabla p \qquad (2.3)$$

U force potential if external forces are conservative F=-∇U. Practically U=gz

Thus

$$\frac{\partial V}{\partial t} - V \wedge \Omega = -\nabla(\frac{p}{p} + \frac{1}{2}V^2 + U) \qquad (2.4)$$

If the movement is rotational zero , $\Omega = 0$ so Φ (x,y,z,t) velocities can be derived

from this potential.

$$V = -\nabla \Phi \qquad (2.5)$$

Equation (2.5) integrated to equation (2.4)

$$\frac{p}{p} + \frac{1}{2}V^2 + U - \frac{\partial \Phi}{\partial t} = C(t) \qquad (2.6)$$

Clearly, Bernoulli equation is obtained as follows

$$\frac{p}{p} + \frac{1}{2}[(\frac{\partial \Phi}{\partial x})^2 + \frac{\partial \Phi}{\partial y})^2 + \frac{\partial \Phi}{\partial z})^2] + gz - \frac{\partial \Phi}{\partial t} = C(t) \qquad (2.7)$$

The given correlation is also neglected if the non-linear $\frac{1}{2}V^2$

$$\frac{p}{p} + g\,\zeta - \frac{\partial \Phi}{\partial t} = C(t) \qquad (2.8)$$

So

$$z = \zeta \text{ for } g\,\zeta - \frac{\partial \Phi}{\partial t} = 0 \qquad (2.9)$$

The free water surface of a wave can be defined as F (x, y, z, t) = η (x, y, t) -z = 0. Where η (x, y, t) free surface z = 0 horizontal is the distance from the plane. If the surface of the free water surface cannot abandon this surface and the normal rate of liquid for each point on the free water surface is assumed to be equal to the surface normal speed, the

5

kinematic water surface boundary condition is defined. This corresponds to equalization of the received derivative to zero following the movement of the free water surface equation. Accordingly, the kinematic water surface requirement;[8]

$$\frac{\partial n}{\partial t} - \frac{\partial \Phi}{\partial x}.\frac{\partial n}{\partial x} - \frac{\partial \Phi}{\partial y}.\frac{\partial n}{\partial y} + \frac{\partial \Phi}{\partial z} = 0 \qquad (2.10)$$

According to the linear theory, the linearized kinematic water surface condition by neglecting the non-linear smaller terms;

$$\frac{\partial n}{\partial t} + \frac{\partial \Phi}{\partial z} = 0 \qquad (2.11)$$

By combining the two equations given as kinematic and dynamic water surface boundary conditions, a single water surface boundary condition can be obtained:

$$\frac{\partial^2 \Phi}{\partial t} + g\frac{\partial \Phi}{\partial z} = 0 \qquad (2.12)$$

If it is assumed that the water is bounded by a horizontal floor at the depth d, the vertical velocity of the liquid along the base must be zero.[8]

$$w = -\frac{\partial \Phi}{\partial z} = 0 \quad \text{on } z = -d \qquad (2.13)$$

2.2 Literature Review

Examination of the wave resistance produced by a moving object close to the free surface can be divided into two parts, which can be defined as breaking and non-breaking wave components [10]. In the case of non-breaking wave, the resistance diffuses away from the body, while breaking wave conditions break the wave energy [11]. Salvesen's[12,13] work in 1966 clearly proved the importance of the effect of nonlinearity at the free surface. Salvesen found that these methods did not calculate sufficient validation, and even in many cases there were differences up to 40-50% and these differences were due to the non-linearity of the effects of non-linear terms. He has proposed linear and second order theoretical methods for the mathematical representation of the problem. Then, he has extended his work for third order theory results. Dawson[11] experimental and numerical into the effect of submergence depth, Froude number and length-to diameter ratio in the among of interactive relation a nearly free surface submerged body. In 1983, Duncan [14] conducted a comprehensive experimental study on

the breaking of waves caused by a two-dimensional hydrofoil, completely submerged in a steady horizontal motion. His experimental work was used to separate the resistance on the hydrofoil into two parts. It was established that at 'incipient breaking' the first wave occurred in either a breaking or non breaking indicate based on the starting situations. In 1991 Çalışal[15] et al have conducted of a numerical ship-wave resistance formulation analysis with an iterative procedure, which accommodates nonlinear free surface conditions, parallel to Gadd's[1] formulation and compared them with the experimental results given by Salvesen. Çalışal's solution was attend to give better results than the first order solution of Salvesen but not as good as the second order solution, if the experimental values are used as a standard for comparison. N. Xie and D. Vassolos [16] developed a panel method to estimate the steady flow around an underwater hydrofoil with a finite aspect ratio under potential flow assumptions. This technique employs constant density pairs and distribution of weld density around the hydrofoil. After obtaining the solution of the pairs on the interface resources, the numerical results of the pressure, lift and resistance coefficients as well as the wave profiles are calculated for different Froude numbers and immersion depths to show the effect of free surface and aspect ratio performance. Y. Uslu and S. Bal [17] examined the hydrodynamic forces, wave elevation properties and the distribution of the pressure around 2 and 3 dimensional bodies by boundary element methods. The boundary element method is a recursive feature initially configured for both 2D and 3D cavity foil shapes, and ship-like bodies moving at or below the free surface at a free constant velocity are applied to a 2-dimensional hydrofoil. Reichl et al [18] using the ANSYS Fluent commercial tool, they investigated the flow through a cylinder near the free surface at Reynolds number 180. Awakening behavior of 0.0-0.7 diameters in immersion rate and Froude numbers between 0.1 and 5.0 diameters were thoroughly investigated. Noteworthy studies include computational modeling of vortex fields among specified parameters that help determine the magnitude of wave conditions. Rhee and Stern [19] examined Duncan's experiments with numerical techniques. The analyzes concluded that fracture waves, which are composed of the effect of dimensional separation and solution area dimensions and which have an unstable wave profile Gretton et al. [20] performed RANS CFD simulations of a submerged foil. For the simulations, NACA 0012 hydrofoil and Froude number 0.567 was used. CFD simulations studied wave elevation and hydrodynamic forces and moments. Due to the unstable nature of the problem at hand, they applied a steady-state solution model, which showed a low concordance with Duncan's findings. Amiri et al. [21] studied simulation of a shallow underwater submarine and

presented the results of drag, lift and pitch moment to determine the interaction between the bow and stern waves of the submarine. Studies include a validation uncertainty amount of the STARCCM + commercial tool used. For this purpose, one of the main objectives of this study is to investigate the wave making properties of a hydrofoil immersed in water with a RANS-CFD-based calculation technique together with the uncertainty quantification procedure. In order to reduce the complexity of the problem to measure uncertainty levels, breaking and non-breaking wave conditions are selected as test cases.. Boucasse et al[22] investigated single phase two-dimensional flow past a circular cylinder piercing, or close to, a free surface at a Reynolds number of 180 by δ-SPH algorithm proposed by Antuono et al.[23,24]where a numerical density diffusive term is adopted into the scheme. They clearly addressed the reasons for modeling the problem in Re = 180 which can be summarized as preventing the 3-d effects on the simulations, resolving all vorticity scales in the flow and last but not the least, the existence of substantial experience led by Reichl and colleagues which suggest to set Reynolds number to 180 for 2-d modeling. In addition to these justifications, Colagrossi et al.[25] recently stated the advantage of low-Reynolds regimes that allows performing simulations without the use of sub-grid models which would increase the complexity of the problem. This work aims to model a similar open-channel flow problem that involves a comparison of an experimental study through a weakly compressible SPH scheme.

2.3. Uncertainty Analysis Procedure

For the quantification of the uncertainty, International Towing Tank Conference [24] recommended procedure 7.5-03-01-01 has been utilized. The main purpose of the ITTC uncertainty quantification procedure determined the error calculation by numerical simulations. A numerical simulation entail adaptation of accuracy the use of a model, and the decoupling of the process by a finite number of elements, time steps, iterations, digits, etc. Verification procedures were extended to include the user options of the correction factor of both safety factors, which were used to estimate numerical errors by section 7 of 23rd ITTC RC Report. In this study, the major uncertainty sources of the numerical simulations performed by RANS methods have been considered as the number of grid elements and time step values which reflect the representation of spatial discretization of

the physical domain and highly unsteady nature of flow evolution.[26]

The procedure is initiated by the convergence studies. The quantification of R_i, namely the convergence ratio is used to assess the convergence of the solution with respect to the refinement of the input parameters in consideration. 3 solutions with the usage of constant refinement ratio R_i is necessary for the process. In this study, convergence of the numerical solutions have been assessed with respect to grid and time step refinement. Changes between medium-fine $\varepsilon_{21} = S_{G2} - S_{G1}$ (2.11) and coarse-medium $\varepsilon_{32} = S_{G3} - S_{G2}$ (2.12) solutions are used to define the convergence ratio.Under the assumption of monotonic convergence ($0 < R_i < 1$) being achieved[27],

$$R_i = \frac{\varepsilon_{i21i}}{\varepsilon_{i32i}} \tag{2.13}$$

Based on the value of obtained R_i, there may occur four conditions[26]:

- $0 < R_i < 1$, monotonic convergence

- $-1 < R_i < 0$, oscillatory convergence

- $R_i > 1$, monotonic divergence

- $R_i < 1$, oscillatory divergence

Under the assumption of monotonic convergence being achieved, the generalized Richardson Extrapolation (RE) estimation is used to find the error, $\delta_{REi1}{}^{*}$, for the selection of ith input parameter and order of accuracy, pi which are defined as follows.[27]:

$$\delta_{REi1}{}^{*} = \frac{\varepsilon_{i21i}}{r_i{}^{P_i} - 1} \tag{2.14}$$

$$p_{i=} \frac{ln(\varepsilon_{i32} - \varepsilon_{i21})}{ln(r_i)} \tag{2.15}$$

where r_i is the uniform refinement ratio which is taken as $\sqrt{2}$ for both grid and time-step solutions. The correction factor which is based on the verification of 1-d wave equation, 2-d Laplace equation and Blasius boundary layer analytic benchmarks recommended by ITTC Procedure is utilized in the uncertainty quantification procedure

Here, pi,est is defined as the estimation for the limiting order of accuracy of the first

term as increment size goes to zero and the asymptotic range is reached ($C_i \rightarrow 1$) which is higher to 1 in the present study.The magnitude of the correction factor derives the rest of the procedure in quantifying the uncertainty U_i.

$$U_i = |C_i \delta_{REi}{}^*| + |(1-C_i)\, \delta_{REi}{}^*|$$

(2.17)

while for $C_i < 1$ the corrected uncertainty, U_{iC} is employed as follows:

$$U_{iC} = |1 - C_i||\delta^*_{RE_{i,1}}|$$

(2.18)

The verification uncertainty may be quantified as below:

$$U_{SN}^2 = U_G^2 + U_T^2 \quad \text{where:}$$

U_{SN}: Verification uncertainty,

U_G: Grid uncertainty,

U_I : Time-step uncertainty.

The validation uncertainty is obtained as follows:

$$U_V^2 = U_{SN}^2 + U_D^2 \quad \text{where}$$

U_V: Validation uncertainty,

U_D : Experimental uncertainty.

3. NUMERICAL ANALYSIS

3.1 Numerical Methodology

In this chapter, this section gives general information of the modeling techniques for RANS simulations. The utilized geometry and the experimental results have been acquired from Salvesen's work . In order to define these methodologies, it is useful to define the geometrical and non-dimensional parameters of the problem. Schematic view of the problem and the dimensions of the hydrofoil are ensured in Figure 3.1 and Figure 3.2. The non-dimensional parameters that represent the physical conduct of the fluid flow are submergence, hydrofoil and channel depth Froude numbers and the Reynolds number in order of which are represent as:

$$Fr_{c=}\sqrt{\frac{U}{gc}} \quad Fr_{D=}\sqrt{\frac{U}{gD}} \quad Re_{=}\frac{Uc}{v} \tag{3.1}$$
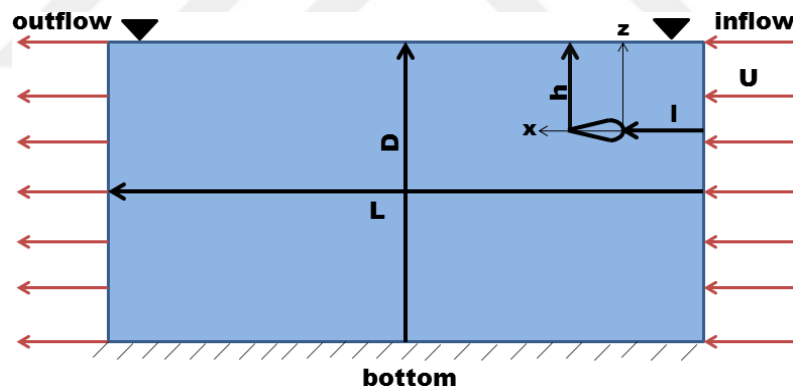

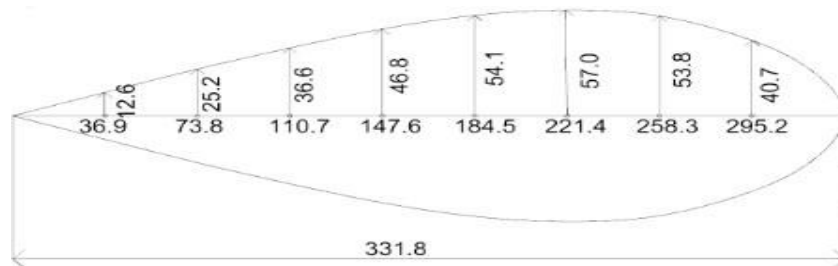**Figure 3.1** Parametric Description of the Channel Geometry

Figure 3.2 Parametric Description of the Foil Geometry

where c denotes the chord length of the hydrofoil. The numerical test matrix is expensed in Table 3.1.

Table 3.1 Numerical Test Matrix

h/D	Fr_c			
0.48	0.55	0.71	0.87
0.57	0.55	0.71	0.87

The hydrofoil geometries ground from Salvasen[12] has been imported to Rhinoceros software and then exported to Ansys Design Modeler for boolean operations and solution domain producing. The meshing operation was then completed by Ansys Mesher. Since the problem is a multi-phase problem, it requires the capture of elevations on the free surface. The expected free surface treatment was achieved with a 20-cell inflation layer in a vertical direction at constant vertical resolution. In connection with the requirements of the turbulence modeling strategy, an inflation layer was also used near the 12 cell hydrofoil and with a growth rate of 1.2. In the uncertainty analysis, the mesh size and cell number used for simulations in consecutive sections will be reported due to changes in free surface and hydrofoil dimensions. Mesh details in way of free-surface and hydrofoil are given in Figures 3.3 and 3.4, respectively.
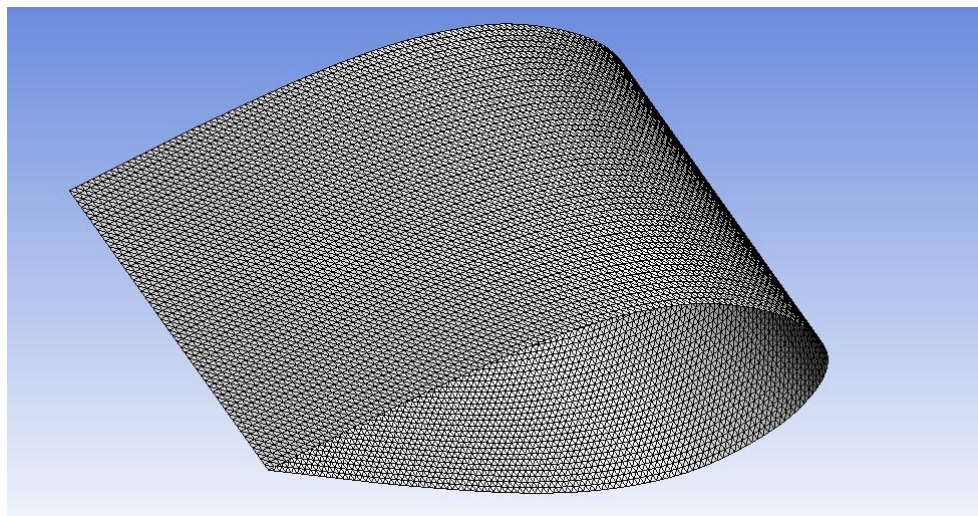
Figure 3.3 Grid Refinement in way of Hydrofoil
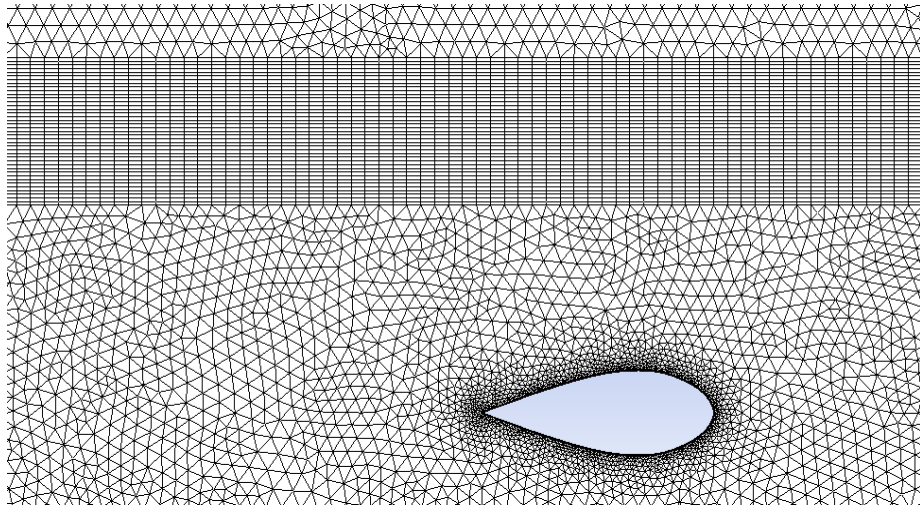
Figure 3.4 Grid Density in way of Free Surface

The analyses have been handled on ANSYS-CFX v14. Volume of Fluid method has been used for the multi-phase modelling. SST k-ω turbulence model has been utilized along with second order solver and turbulence numerics. The boundary conditions used are depicted in Figure 3.5. Due to the symmetric nature of the problem, half model has been utilized.
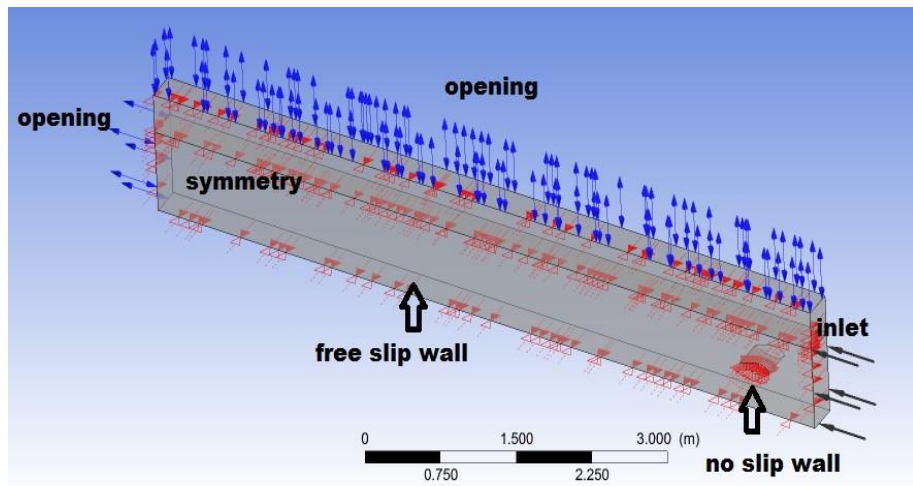
Figure 3.5 The Utilized Boundary Conditions in RANS Modelling

Prior to the actual analysis, a grid independence study was planned according to ITTC's methodology. [26]. The hydrofoil has been analyzed at h/D=0.48 depth for Fr_c =0.87. For the expected free surface area, 5 different grids with different mesh sizes were prepared. A grid independent solution in terms of maximum wave amplitude has been obtained with the third solution, with a total of 1,258,499 elements. The variation of maximum wave amplitude with number of cells is given in Figure 3.6.

Figure 3.6 Variation of wave amplitude with mesh density

3.2 Validation of Free-Surface Deformations

The wave profiles approximations of the submerged hydrofoil by RANS methods have been handled at two submergence depth and three Froude numbers. The wave profiles obtained by RANS CFD numerical techniques have then been collated with Salvesen's experimental results and first and second order theory solutions. As mentioned earlier, the main purpose of validation is to investigate the ability of 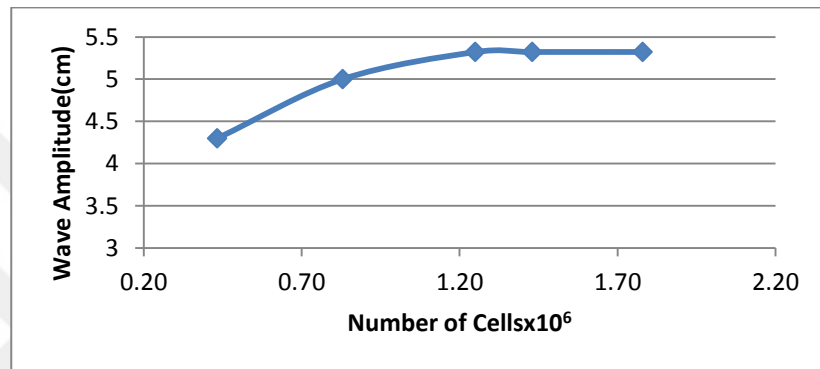the numerical technique to capture the waves generated by the submerged hydrofoil. Comprehensive care has been taken in RANS simulations to prevent back-pressure effects caused by channel length. Initial computations indicated that utilization of small channel lengths (approximately 12 chord lengths from the trailing edge) resulted in an unsteady wave profile, which then was found out to be purely of numerical nature. This numerical instability was captured to occur during the formation of successive wave crests; the latter crests affecting the wave amplitude and longitudinal position of the first crest. The induced wave profile, especially at high speed cases has been seen to be of unsteady nature; this being confirmed by the disagreement between the experiments and initially conducted steady state RANS solutions. Using the unsteady solver, it was possible to capture the experimental wave profiles after a solution time of 20 seconds.. Results are given for h/D=0.48 in Figures 3.7 a, b and c and for h/D=0.57 in Figures 3.8 a, b and c respectively .
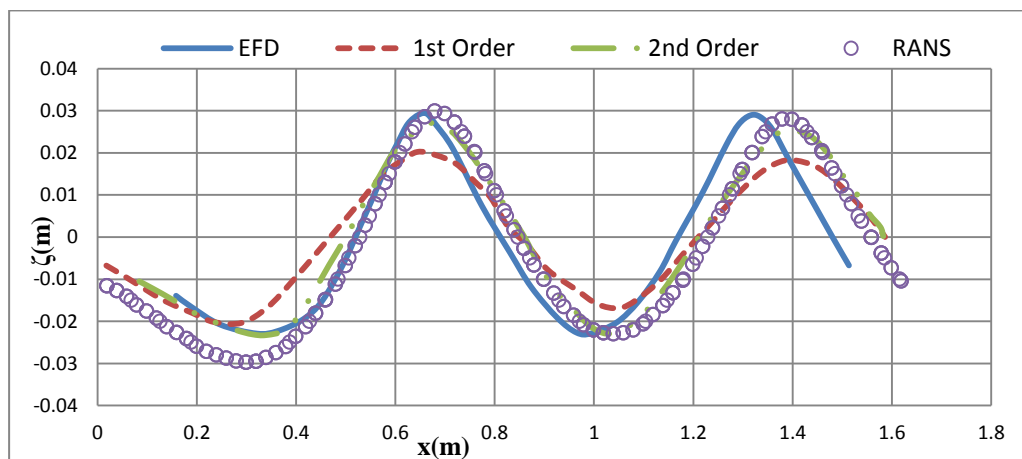

Figure 3.7 (a)
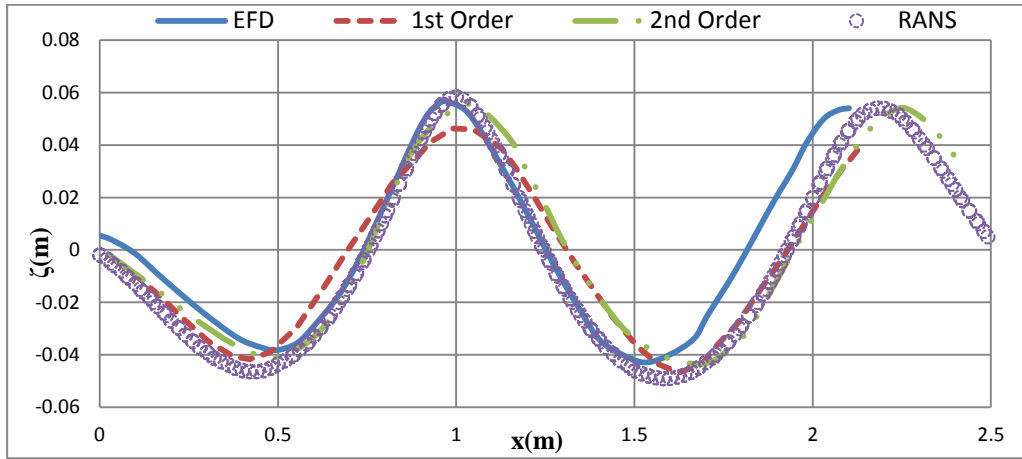
Figure 3.7 (b)
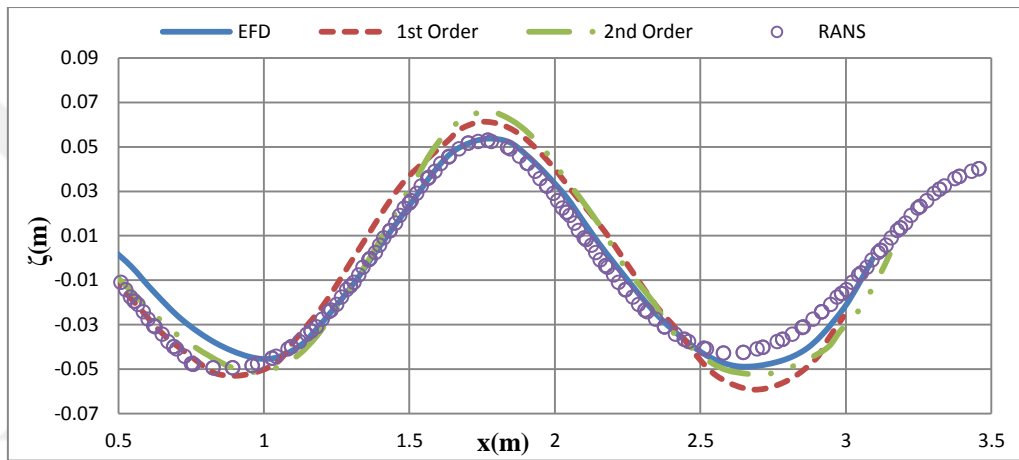
Figure 3.7 (c)

Figure 3.7 : Wave profiles for h/D=0.48 (a) Fr_c =0.55 (b) Fr_c =0.71 (c) Fr_c =0.87

Figure 3.8 (a)

16
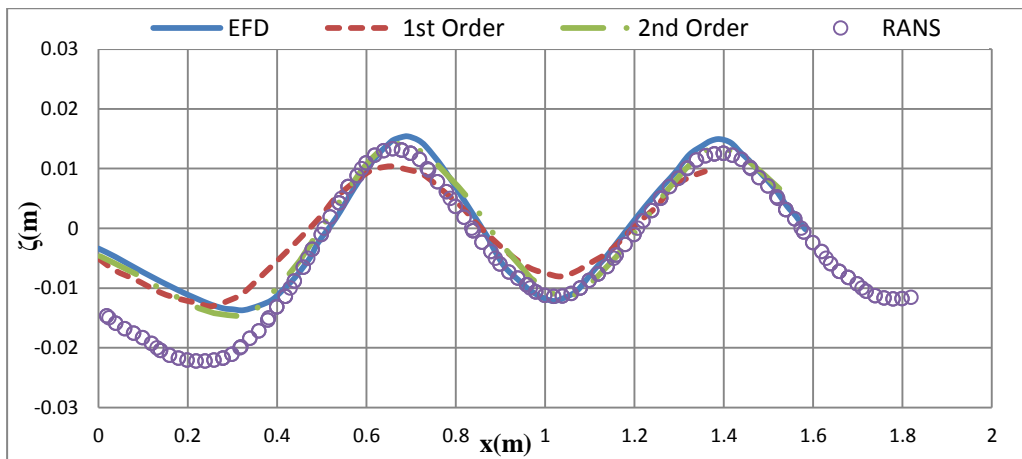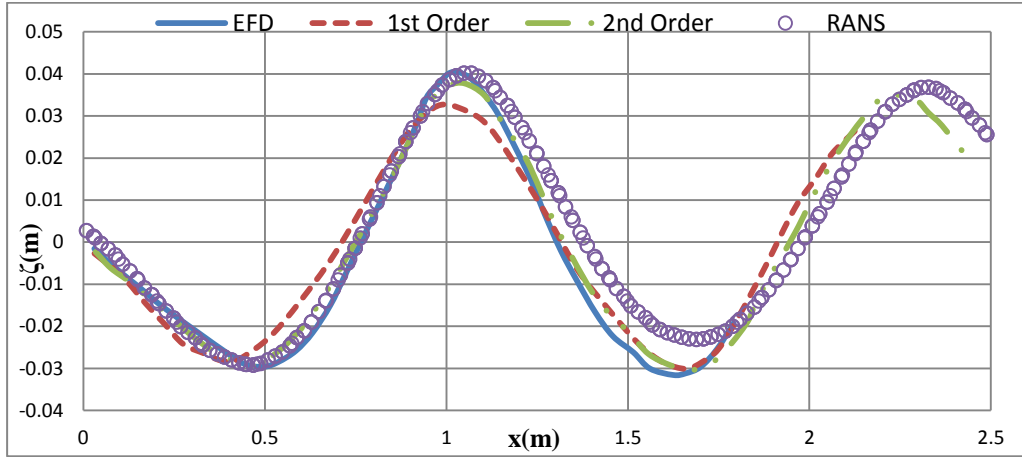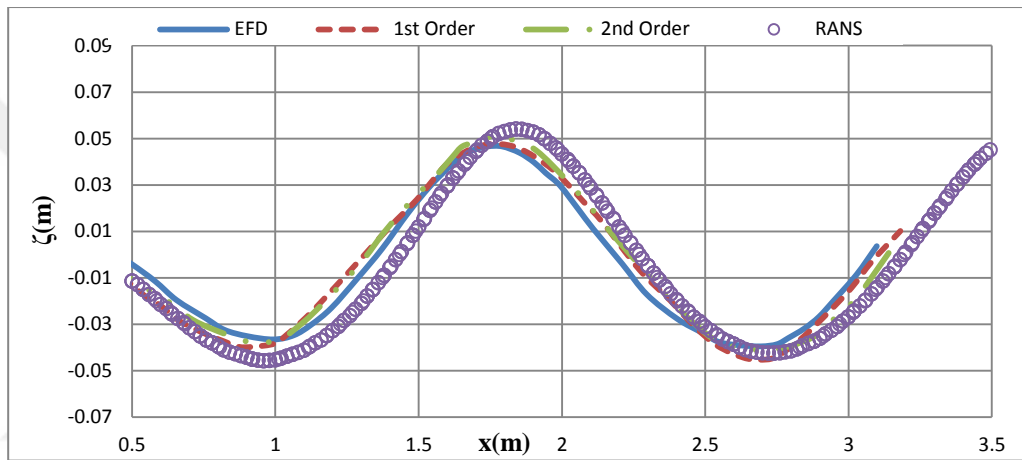
Figure 3.8 (b)

Figure 3.8 (c)

Figure 3.8 : Wave profiles for h/D=0.57 (a) Fr_c =0.55 (b) Fr_c =0.71 (c) Fr_c =0.87

Differences in numerical approaches require different modeling strategies, as seen in channel length determination. This also applies to defining the channel depth; Defining the free slip condition at the bottom of the channel allows the use of a less deep channel at an additional cost to ensure that the modeled problem does not suffer from shallow water effects. It is important to note that the simulations are performed for two submergence levels at constant depths (D) of the channel and it has been investigated that the use of higher depth values does not alter the free surface profiles. It is caused by the lower wall boundary to keep the mesh members within an acceptable range with avoidance of grounding effects, with an optimum D = 800mm being observed to ensure sufficient accuracy in the results for each immersion level of the profile. results for each submergence levels of the profile.

3.3 Validation of Wave Resistance and Hydrodynamic Performance of Submerged Hydrofoil

In Salvasen's studies, wave resistance has been obtained during the model tests by a prescribed method. In Salvasen's methodology, the horizontal drag at low submergence condition has been subtracted from the horizontal drag of the 1.371 [m] submerged condition, under the assumption that the total resistance at the deeply submergence condition is of viscous nature.

In this study, wave resistance was obtained by RANS simulations using the prescribed Salvesen method. Simulations have been handled for the deeply submerged case h/c = 4.129 and at a submergence of h/c = 1.148 for the Fr_c numbers given in Table 3.2. As a result, wave resistance data has been acquired numerically and results are shewed in a comparative way along with experimental data in Figure 3.8 where fine mesh and time-step values of uncertainty analysis is utilized. The agreement between experimental and numerical results is excellent.

Table 3.2 RANS Wave Resistance [N] Comparison with Salvesen(1969)

Fr_c	EFD	RANS	Error (%)
0.506	0.3296	0.3440	4.37
0.591	0.7396	0.7581	2.50
0.676	1.3554	1.3863	2.28
0.760	1.8611	1.8996	2.07
0.844	2.0618	2.0931	1.52
0.929	1.9392	1.9656	1.36
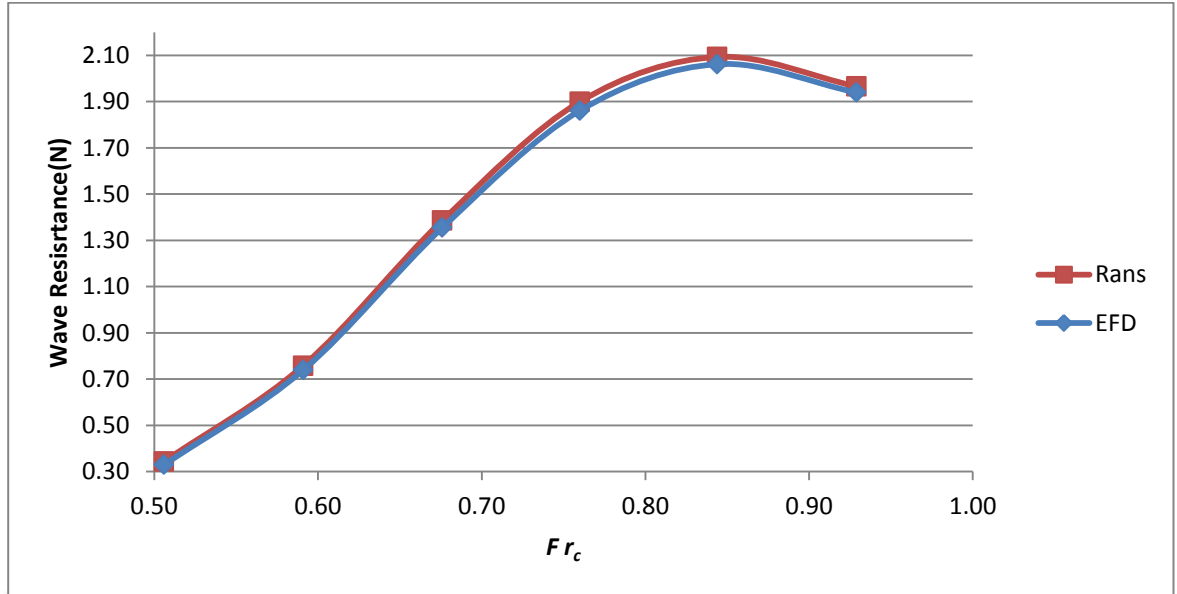
Figure 3.8 : Validation of wave resistance results of RANS and EFD

The hydrodynamic performance of the hydrofoill was investigated for the entire velocity range; the immersion rate of h / c = 1,148 ,Froude numbers are between 0.506 and 0.929. Results are indicated the form of drag and lift coefficients Froude number in Figure 3.9. The non-dimensional drag and lift coefficients are obtained as:

$$C_{D=\frac{D}{0.5pSU^2}} , \qquad C_{L=\frac{L-F_b}{0.5pSU^2}}$$

(3.1)

where F_b is the initial buoyancy force and S indicates the planform area in RANS method. When the buoyancy force is derived from total force in the vertical direction, there is a small force component resulting from changes in the pressure of the edges of the hydrofoil resulting from the deformation of the free surface. This force component increases with decreasing Froude numbers, the effect is best seen from the free surface deformations given in figures 3.6 and 3.7.
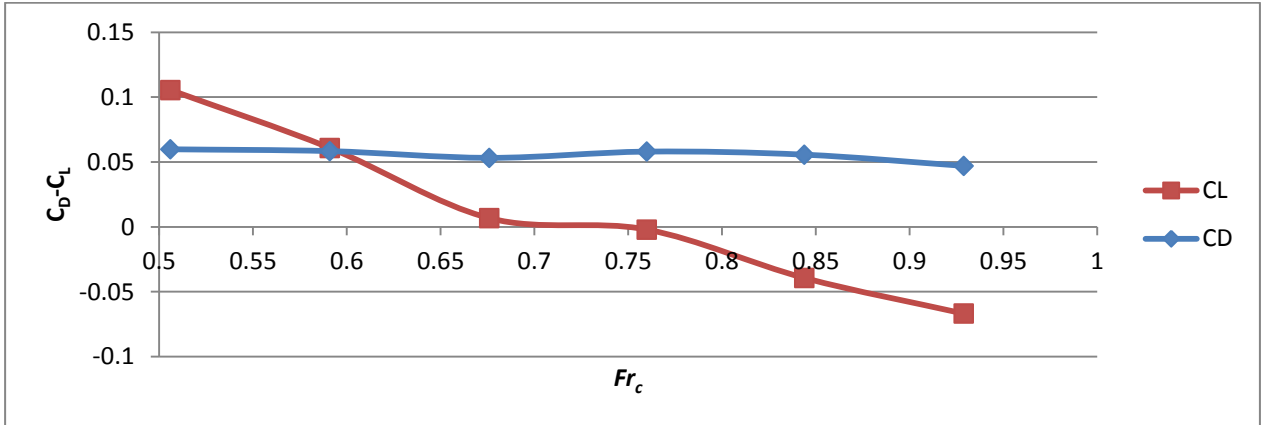
Figure 3.9 : RANS solutions of lift and drag coefficients in different Fr_c number flow regimes

3.4 Uncertainty Analysis

The uncertainty of the free surface deformations obtained in the absence of cavitation and wave break events and the wave resistance uncertainty analysis affecting the hydrofoil are one of the main objectives of this study. Uncertainty levels in wave profile estimation and uncertainty analysis in wave resistance in RANS CFD method. In the following subsections, the details of the uncertainty analysis information will be given.

3.4.1 Wave Profile Uncertainty Analysis

The uncertainty of in the prediction of wave profile for by RANS numerical techniques have been completed as per quantified for the h/D=0.48 submergence ratio and Fr_c=0.71. Unsteady nature of the wave making problem have an unsteady nature in the analyzed velocity and immersed ratio should be surveyed. Therefore, the wave making problems has been solved in an unsteady solved fashion with for RANS numerical techniques. Numerical simulations are calculated depending on time and the a total time in simulations was taken as of 20 seconds has been set for the simulations, enabling the wave profile to fully develop and enable the decay of initial transient effects. The average amplitude of first wave crest heights occurring beyond the trailing edge of the profile is calculated to obtained used in order to quantify the wave profile uncertainty. Owing to the unsteady nature of the problem, amplitude data obtained at each acquired time step is then

averaged to obtain a final solution. The data acquisition frequencies are 0.25 (s) for RANS simulations respectively.

RANS numerical simulations are defined by using the ITTC CFD Verification and Validation procedure has been used for the uncertainty analysis[26]. Results are acquired for 3 different grids and 3 different time steps with 6 data points for both numerical methods with uniform refinement ratio $r_G=\sqrt{2}$. Total number of elements and time step details given in table x and table y. The first wave crest heights solutions are expressed with three set of grids S_{G1}, S_{G2}, S_{G3} and three set of time steps S_{T1}, S_{T2}, S_{T3} details given in Table 3.3 and Table 3.4.

Table 3.3 Total number of grid elements and time step values [s] in RANS wave profile uncertainty simulations.

	Number of Grid Elements			Time Step		
	Fine	Medium	Coarse	Fine	Medium	Coarse
RANS	2028851	1139151	716329	0.007	0.01	0.014

Table 3.4 First wave crest heights (cm) obtained from variable grid and time step values of RANS simulations where the experimental data is given as 5.66 (cm)

	Fine	Medium	Coarse
Grid	5.69	5.59	5.13
Time-step	5.68	5.69	5.85

The necessary coefficients for wave profile uncertainty calculation of RANS is given in Table 3.5 and 3.6. In these tables, R_i stands for convergence rate, P_i for order of accuracy, C_i for correction factor, U_i for network uncertainty, σ_{i1}^* for error, U_{iC} for corrected uncertainties, and simulation value S_i is the validation of wave amplitude.

Table 3.5 Grid and Time-step Verification of Wave Profile for RANS Simulations

	R_i	p_i	C_i	U_i	σ_{i1}^*	U_{iC}	S_i
Grid	0.2250	4.3046	3.4454	0.00177	0.00103	0.00073	0.0569
Time-step	0.0867	7.0559	10.535	0.00026	0.00014	0.00013	0.0568

In order to assess validity of a numerical solution, uncertainty U_V is determined from numerical uncertainty U_{SN} and experimental uncertainty U_D. To achieve validation, the comparison error $|E|$ must be smaller than the validation uncertainty. In Salvesen's

study, it has been reported that the experimental setup enabled the measurement of the wave height with an influence on the results at a magnitude of 0.03 inches. As the procedure followed for obtaining this value is not evident in Salvesen's text, the 0.03 inches value declared by Salvesen has been assumed as the uncertainty of the experiment arising from the measurement system during this study

Table 3.6 Validation of Wave Profile RANS Simulations

$|E|$	U_V	U_D	U_{SN}	Relation
1.56E-4	1.94E-3	7.62E-4	1.79E-3	$|E| < U_V$
0.28%	3.42%	1.35%	3.15%	$|E| < U_V$

3.4.2 Wave Resistance Uncertainty Analysis

In this study, the uncertainty of RANS method in estimating wave resistance has been quantified for the hydrofoil at a submergence ratio of h/c = 1.148 and at a flow velocity of Fr_c = 0.76. Details of wave resistance calculation methodology have been explained in chapter 3.3. The procedure requires the uncertainty quantification to be investigated by a set of 3 grids and a set with 3 different time steps with a uniform refinement ratio, taken as $r_G=\sqrt{2}$. The number of divisions along the foil has been changed in assessing the effect of grid refinement. Solutions denoted as fine, medium and coarse grid correspond to namely S_{G1}, S_{G2}, S_{G3} and time steps S_{T1}, S_{T2} and S_{T3} where the values are tabulated in Table 3.7. The verification of wave resistance coefficients details are shown in Tables 3.8 and 3.9.

Table 3.7 Total number of grid elements and time step values [s] in RANS wave resistance uncertainty simulations

	Number of Grid Elements			Time Step		
	Fine	Medium	Coarse	Fine	Medium	Coarse
RANS	2155922	2028851	1966980	0.007	0.01	0.014

Table 3.8 Wave Resistance [N] results obtained from variable grid and time-step values of RANS simulations where the experimental data is given as 1.8611 [N]

	Fine	Medium	Coarse
Grid	1.9198	1.9370	2.0271
Time-step	1.8996	1.9198	2.1325

Table 3.9 Grid and Time-step Verification of Wave Resistance for RANS Simulations

	R_i	P_i	C_i	U_i	σ_i^*	U_{iC}	S_i
Grid	0.1905	4.7848	4.2504	0.0303	0.0172	0.0131	1.9198
Time-step	0.0950	6.7928	9.5297	0.0383	0.0202	0.0181	1.8996

Validation has been assessed by evaluating the effect of grid convergence and time-steps, enabling the quantification of numerical uncertainty, namely U_{SN} where details are given in Table 3.10. In Salvesen's study, any evaluation on the sources of errors or uncertainties regarding wave resistance has not been reported. Although this prevents the quantification of the experimental uncertainty U_D, the comparison error as in the case of wave height evaluation- is smaller than the numerical uncertainty; resulting in a case in which the solution was able to be validated even in the absence of experimental levels of uncertainty.

Table 3.10 Validation of Wave Resistance RANS Simulations

$|E|$	U_V	U_D	U_{SN}	Relation
3.85E-2	4.88E-2	N/A	4.88E-2	$|E| < U_{SN}$
2.07%	2.60%	N/A	2.60%	$|E| < U_{SN}$

4. DISCUSSIONS

When the experimental results are compared with the wave profiles determined by the calculations, it is seen that the wave profiles and numerical results generated by the hydrofoil immersed from the experimental study are in agreement with the inflow rate. At low speeds, the initial agreement between wave amplitudes tends to deteriorate along the channel. The same result is valid for first and second order theory results. Since the magnitude of the wave amplitude is at the level of two centimeters at the lowest speed cases, the experimental uncertainties are expected to reach relatively significant levels compared to the high speed cases. With increasing depth, very consistent results are obtained with numerical tools. It starts to deteriorate along the channel.

In low Froude numbers, the RANS numerical method captures the position and amplitude of the first peak and has a good fit towards the second peak. The longitudinal position of the second peak is slightly missed by numerical methods including first and second order theories. RANS method best captures the amplitude of the second peak.

At moderate Froude numbers, similar results were obtained. RANS estimates are in good agreement with experiments with only a slight deviation in the longitudinal position of the second peak. RANS results are also superior to first and second order theories. At the Froude numbers, the RANS results capture the entire wave profile and are in perfect agreement with the experiments.

It is also worth mentioning that at high speeds, transient effects are captured by numerical techniques. In high-speed cases, the induced wave has been found to be unsteady; this is confirmed by disagreements between experiments and the steady state RANS solution. Using the unsteady solvent, it was possible to capture the experimental wave profile after a certain solution time and a repetitive wave profile change was observed.

At lower Froude numbers, the induced wave system is initiated with a trough which originates approximately from the leading edge; as Fr increases this effect diminishes and the trough is shifted from x = 0.5[m] to x = 1.0[m]. This results in a downward force coefficient, captured by RANS numerical technique.

In addition, it was found that the previously mentioned assumption about the value of experimental uncertainty does not affect the validity of numerical methods for the situation in this question. Since the magnitude of the error in the wave amplitude is less than the numerical uncertainty analysis; it can be said that the RANS method may be verified even if there is no experimental uncertainty value.

The agreement between experimental and numerical results in terms of wave resistance is excellent; the percentage of error is less than two percent at high speeds at which the wave resistance component begins to dominate. The higher error percentage observed in the lowest Frc number is attributed to the fact that the wave resistance is lower in order of magnitude compared to viscous resistance.

5. CONCLUSIONS

The flow around a immersed hydrofoil has been investigated by a commercial RANS CFD package. Effect of submergence depth and Froude number on the induced wave profile has been investigated. The analyzed case has been based on Salvesen's experimental work, enabling validation of numerically obtained results.

The agreement achieved between the wave profiles near the vicinity of the trailing edge at lower speeds tend to deteriorate with the progression of the flow towards the channel outlet.

The agreement of wave profiles at higher speeds   between experimental data and numerical results are   improved substantially.   RANS CFD and experimental results show an excellent agreement in wave amplitude.

 The uncertainties of RANS method in predicting free-surface deformations have been quantified, and the solutions obtained from RANS method have been validated according to 28th ITTC 2017 recommended procedure 7.5-03-01-01. The magnitude of error in capturing the wave profiles associated with RANS method are below the numerical uncertainties; enabling the validation of RANS method even in the absence of experimental uncertainty values.

Salvesen's experimentally obtained wave resistance values have been compared to those obtained by RANS CFD. The numerical uncertainty has also been quantified and RANS CFD results of wave resistance have been validated. The numerical error in wave resistance was found to be less than the numerical uncertainty as in the case of wave profile enabling the validation of the results even in the absence of experimental uncertainty values.

During the quantification of the uncertainty of RANS calculations, it has been seen that the major component of uncertainty associated with the prediction of wave profile arises from grid sensitivity which is approximately one order of magnitude larger compared to the contribution from time-step sensitivity. In the case of wave resistance analysis in RANS CFD, both factors contribute at similar orders of magnitude.

REFERENCES

[1] Gadd, G., 1976. A method for computing the flow and surface wave pattern around full forms. Transactions of Royal Institution of Naval Architects 118, 207–18.

[2] Calisal, S., Goren, O., Okan, B., 1991. On an iterative solution for nonlinear wave calculatons. Journal of Ship Research 35, 9–14.

[3] Dawson, C., 1977. A practical computer method for solving ship-wave problems, in: Second International Conference on Numerical Ship Hydrody- namics, California, USA. pp. 30–8.

[4] Ozbulut, M., 2013. Investigation of Violent Free Surface Flows by SPH Method (in Turkish). Ph.D. thesis. Istanbul Technical University, Institute of Science and Technology.

[5] Reichl, P., Hourigan, K., Thompson, M., 2003. The unsteady wake of a circular cylinder near a free surface. Flow, Turbulence and Combustion 71, 347–59.

[6] Liu, M., Liu, G., 2010. Smoothed particle hydrodynamics: An overview and recent developments. Arch. Comput. Methods Eng. 17, 25–76.

[7] Boucasse, B., Colagrossi, A., Marrone, S., Souto-Iglesias, A., 2014. Viscous flow past a circular cylinder below a free surface, in: ASME 2014 33rd Int. Conf. on Ocean, Offshore and Arctic Engineering OMAE2014, San Francisco, California, USA. pp. 24488–97.

[8] Sabuncu, T. Gemilerin Dalga Direnci Teorisi, İstanbul Teknik Üniversitesi, Gemi Enstitüsü Bülteni, Eğitim Neşriyatı No.1, No. 12, İstanbul,1962.

[9] https://ocw.mit.edu/courses/mechanical-engineering/2-016-hydrodynamics-13-012-fall-2005/readings/2005reading7.pdf

[10] Froude, W., Abell, W., Gawn, R., Duckworth, A., of Naval Architects, I., 1955. The Papers of William Froude, 1810-1879. With a Memoir by Sir Westcott Abell and an Evaluation of 29 William Froude's Work by R.W.L. Gawn : Collected Into One Volume. Institution of Naval Architects

[11] Dawson, C., 1977. A practical computer method for solving ship-wave problems, in: Second International Conference on Numerical Ship Hydrody- namics, California, USA.

pp. 30–8.

[12] Salvasen, N., 1966. On second-order wave theory for submerged two- dimensional bodies. Ph.D. thesis. University of Michigan.

[13] Salvesen, N., 1969. On higher-order wave theory for submerged two- dimensional bodies. Journal of Fluids Mechanics 38, 415–32.

[14] Duncan, J., 1983. The breaking and non-breaking wave resistance of a two- dimensional hydrofoil. Journal of Fluids Mechanics 126, 507–20.

[15] Calisal, S., Goren, O., Okan, B., 1991. On an iterative solution for nonlinear wave calculatons. Journal of Ship Research 35, 9–14.

[16] Xie, N. Vassalos, D. (2007). Performance Analysis of 3D Hydrofoil Under Free Surface, Ocean Engineering 34(8-9):1257-1264.

[17] Uslu, Y. and Bal, S. (2008) Numerical Prediction of Wave Drag of 2-D and 3-D Bodies under or on a Free Surface, Turkish Journal of Engineering and Environmental Science, 32:177-188.

[18] Reichl, P., Hourigan, K., Thompson, M., 2005. Flow past a cylinder close to a free surface. Journal of Fluid Mechanics 533, 269–96.

[19] Rhee, S.H.,Stern, F., (2002) RANS Model for Spilling Breaking Waves, Journal of Fluids Engineering, 124: 424-432

[20] Gretton I., Bryden I.,Couch J., and Ingraml, M .(2010) The CFD Simulation of a Lifting Hydrofoil in Close Proximity to a Free Surface, International Conference on Ocean, Offshore and Artic Engineering, June 6-11,2010

[21] Amiri, M., Esperanca, P., Vitola, M., Sphaier, S., 2018. How does the free surface affect the hydrodynamics of a shallowly submerged submarine? Applied Ocean Reseach 76, 34–50.

[22] Boucasse, B., Colagrossi, A., Marrone, S., Souto-Iglesias, A., 2017. Sph modelling of viscous ow past a circular cylinder interacting with a free surface. Computers and Fluids 146, 190–212.

[23] Antuono, M., Colagrossi, A., Marrone, S., Molteni, D., 2010. Free surface flows solved by means of sph schemes with numerical diffusive term. Computer Physics Communications

181, 532–49.

[24] Antuono, M., Colagrossi, A., Marrone, S., 2012. Numerical diffusive terms in weakly-compressible sph schemes. Computer Physics Communications 183, 2570–80

[25] Colagrossi, A., Nikolov, G., Durante, D., Marrone, S., Souto-Iglesias, A., 2019. Viscous ow past a cylinder close to a free surface: benchmarks with steady, periodic and metastable responses, solved by meshfree and mesh- based schemes. Computers and Fluids 181, 345–63.

[26] Stern, F., Wilson, R., Shao, J., 2006. Quantitative v & v of cfd simulations and certification of cfd codes. International Journal of Numerical Methods in Fluids 50, 1335–55.

[27] ITTC – Recommended Procedures and Guidelines (2008) Uncertainty Analysis in CFD Verification and Validation Methodology and Procedures